

Inter-Pulse Coding and Coherent-on-Receive Modifications of Magnetron-Based Marine Radar – Experimental Results

Erez Ben-Yaacov¹, Daniel Quartler², and Nadav Levanon²

¹Elisra Ltd, ²Tel Aviv University

Abstract — Magnetron-based, low-cost marine radar was modified. In the transmitter the pulse repetition interval (PRI) was coded periodically. In the receiver a “coherent-on-receive” detection option was added. The coding allows extension of the unambiguous delay (range) beyond the nominal PRI. The added option of coherence allows comparison between coherent and non-coherent integration of many pulses. Experimental results are presented.

Index Terms — Coherent-on-receive, magnetron, marine radar, PRI coding, un-ambiguous range, waveform.

I. INTRODUCTION

Typical magnetron-based civil marine radar adjusts the pulse repetition interval (PRI) and the pulse-width (PW) according to the range setting. For example, in the Furuno 1623, when the maximal displayed range is 1.37 km: PRI=0.33ms and PW=0.08 μ s. While for its maximal displayed range of 29km: PRI=1.7ms and PW=0.8 μ s. Such an adjustment maintains (within a factor of two) the average transmitted power. The corresponding unambiguous ranges are 50km and 250km respectively. In the long distance mode there is additional increase of the energy on target by slowing the antenna rotation rate.

The main penalty of the wider pulse is a tenfold increase in the radial resolution, hence also a tenfold increase of the clutter return (surface and precipitation). With a 6.2 degree horizontal beam-width, a target at 5 km has to compete with 16 acre clutter area (= 65 dunam).

Coherent radar can separate pulse-width from delay resolution by using pulse compression. It does so by transmitting frequency-modulated or phase-coded pulses. Magnetron pulses do not have this capability. Furthermore, coherent integration of M pulses improves the received signal-to-noise (SNR) by a factor of M , while in non-coherent integration the improvement is proportional to \sqrt{M} . Still, magnetron-based radar dominates the civil marine application due to the low cost of producing high microwave power. The issue of Doppler and moving target indication (MTI) is of less significance because of the nature of sea clutter, and low speed or stationary nature of its typical targets.

The performed modifications were intended to enable using the “narrow pulses and short PRI” mode at all ranges, and avoid the reduced unambiguous range by coding the PRI. The “coherent-on-receive” modification was intended to study the SNR gain contributed by coherent integration, important when detecting small targets. Note that when target fluctuations spoil the coherence, coherent integration may cause SNR loss rather than gain. Also, meaningful target velocity requires integration employing fast Fourier transform (FFT) to account for a Doppler shift.

II. TRANSMITTED AND REFERENCE WAVEFORMS

The PRI coding follows the proposal in [1]. A basic uniform pulse train is coded periodically by not transmitting some of the pulses. This “On-Off-Keying” (OOK) is based on Manchester coding of periodic binary sequences that exhibit ideal periodic cross-correlation with a corresponding sequence, stored numerically in the receiver. Two types of periodic sequences were transmitted in the field trials. One is based on Barker 4 (Table 1 and Fig. 1) and the other on Ipatov 5 (Table 2). A “0” in the transmitted sequence row implies an omitted pulse. In the receiver three different reference sequences were tested. Each produces a different response (i.e., periodic cross-correlation output). For the Barker 4 case the three responses are shown in Fig. 2. Note how the unambiguous delay increased from one PRI to 8*PRI. The responses were obtained by cross-correlating the real transmitted pulses with the reference pulses. That response applies to the radar because the received pulses are envelope detected (non-coherent), hence look like the transmitted pulses (excluding attenuation, fluctuations and noise).

Table 1. Trans. and ref. inter-pulse coding based on Barker 4

Pulse #	1	2	3	4	5	6	7	8
Trans.	0	1	1	0	1	0	1	0
Ref. 1	-1	1	1	-1	1	-1	1	-1
Ref. 2	-0.5	1.5	0.5	-0.5	0.5	-0.5	0.5	-1.5
Ref. 3	-0.75	1.25	0.75	-0.75	0.75	-0.75	0.75	-1.25
Ref. NC	0	1	1	0	1	0	1	0

The logic behind the three coded references is as follows. The output response corresponding to targets is always positive; hence only positive output is displayed to the user. There is no way to avoid at least two negative response sidelobes per period. Using Ref. 1 the negative sidelobe of concern appears at a delay equal to the PRI. Therefore the strong direct reception and strong near-clutter will create a “hole” in the response at a delay equal to the PRI and slightly further. The depth of the “hole” is half the height of the direct reception and the near-clutter. True targets at that delay are likely to be weaker hence buried in that “hole” and not seen. There is therefore a motivation to push that “hole” farther away and make it shallower. Ref. 2 achieves that. Under ideal conditions, in which all the transmitted pulses have identical amplitude; the response attained with Ref. 2 will be optimal. In practice, the transmitted pulses are not identical. When the PRI is reduced considerably below its original value, the magnetron pulses tend to change amplitude in some relation to the pause they follow.

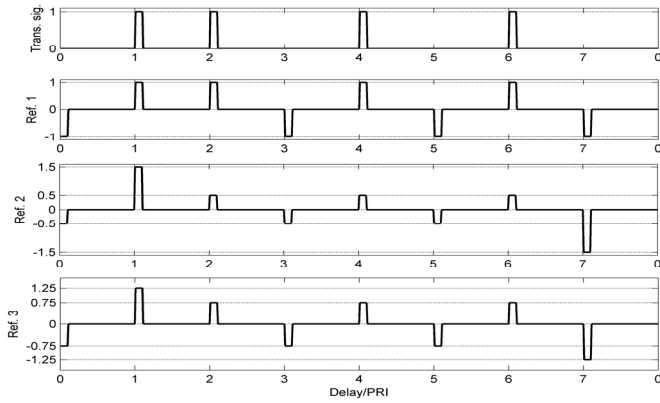


Fig. 1. Trans. and ref. inter-pulse coding based on Barker 4.

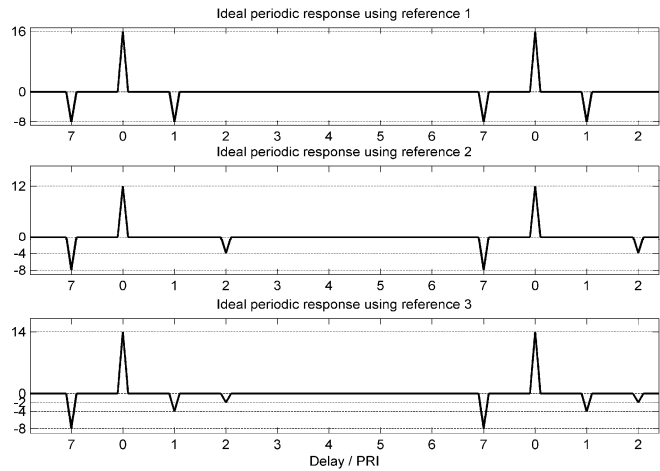


Fig. 2. Ideal periodic responses using the Braker-based signal and its 3 references.

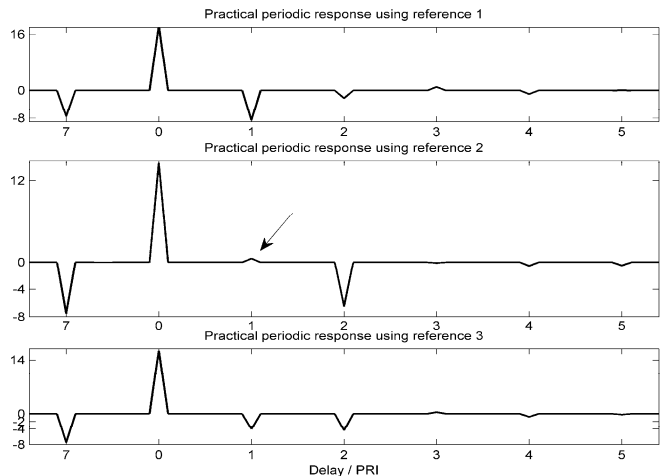


Fig. 3. Practical periodic responses (non-uniform pulses) using the Braker-based signal and its 3 references.

Table 2. Trans. and ref. pulse coding based on Ipatov 5

Pulse	1	2	3	4	5	6	7	8	9	10
Trans.	1	0	1	0	1	0	0	1	1	0
Ref. 1	1	-1	1	-1	1	-1	-2	2	1	-1
Ref. 2	0.5	-0.5	0.5	-0.5	0.5	-2	-1	2.5	0.5	-0.5
Ref. 3	0.75	-0.75	0.75	-0.75	0.75	-1.75	-1.25	2.25	0.75	-0.75

The variable pauses cause the ideal response, shown in the middle subplot of Fig. 2, to change to a response like the one shown in the middle subplot of Fig. 3. The positive sidelobe at the PRI (marked by the arrow) is the most bothersome. It will cause the direct reception and near-clutter to reappear as positive sidelobes around that delay. Even when attenuated by 50 or 60dB, they still are of similar intensity to expected true targets at that delay. The ideal response of Ref. 3 exhibits two shallow negative holes at PRI and 2*PRI (see Fig. 2, lower subplot). Those sidelobes will remain negative despite pulse intensity fluctuations.

Thus, direct reception and near-clutter are not expected to be replicated at a delay equal to the PRI. Note that the above discussion applies also to the Ipatov-based coding, outlined in Table 2. Ref. NC in Table 1 is the reference used in the non-coherent integration. It is identical to the transmitted sequence.

III. EXPERIMENTAL RESULTS

The field trials were conducted with a Furuno 1623 low-cost (< 1500 US\$) civil marine radar. The radar was slightly modified to provide control of pulse triggering and to extract the IF output. The radar operates at X-band (9.41 GHz). It has a 15" antenna, providing 6.2 degree horizontal beam-width. The peak pulse power is 2.2kW. We mainly used the narrow pulses (0.08 μ s). At that pulse-width the antenna rotation rate is 41 rpm. Thus a point target is illuminated for 25ms every 1.46s. At a nominal PRF of 6250Hz, the 8 pulse positions in a period occupy 1.28ms, namely, the target illumination contains approximately 19 code periods or 72 transmitted pulses. This is therefore the length of the reference sequence. Hamming weight multiplies the reference sequence. 240 pulses are integrated when the highest (20kHz) PRF is used.

A. Tel Baruch Field Test

In this field trial the radar was located on a cliff at the sea shore, north of Tel Aviv. The only sea targets were very small fishing or pleasure boats. The purpose of this experiment was to study and compare the nature of the detected and integrated background (noise and clutter) and targets. The transmitted pulses followed the Ipatov 5 sequence (Table 2). Three detection modes were performed simultaneously: Coherent-on-receive, non-coherent, and our new type of processing, in which Reference 1 of Table 2 was used.

Outputs from the three detection approaches, when detecting a small boat, are shown in Fig. 4. The intensities follow the expected probability density functions (PDFs). The PDF of integrated noise following non-coherent and coherent integration are well known. With regard to our "Ipatov" type of processing, note that the reference sequences exhibit zero average. When such a sequence is cross-correlated with envelope detected noise (always positive) the correlation output has zero mean too. As shown in [2], when many periods are non-coherently integrated the noise-only output's PDF approaches a zero-mean Gaussian density. This is in contrast to conventional non-coherent integration of noise.

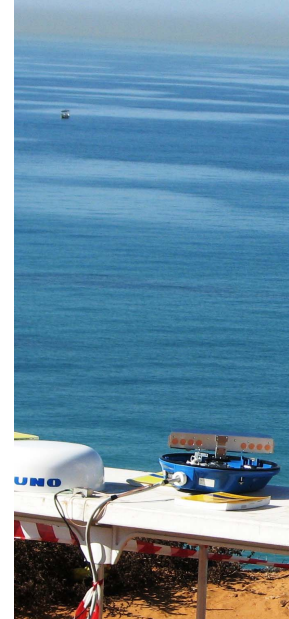
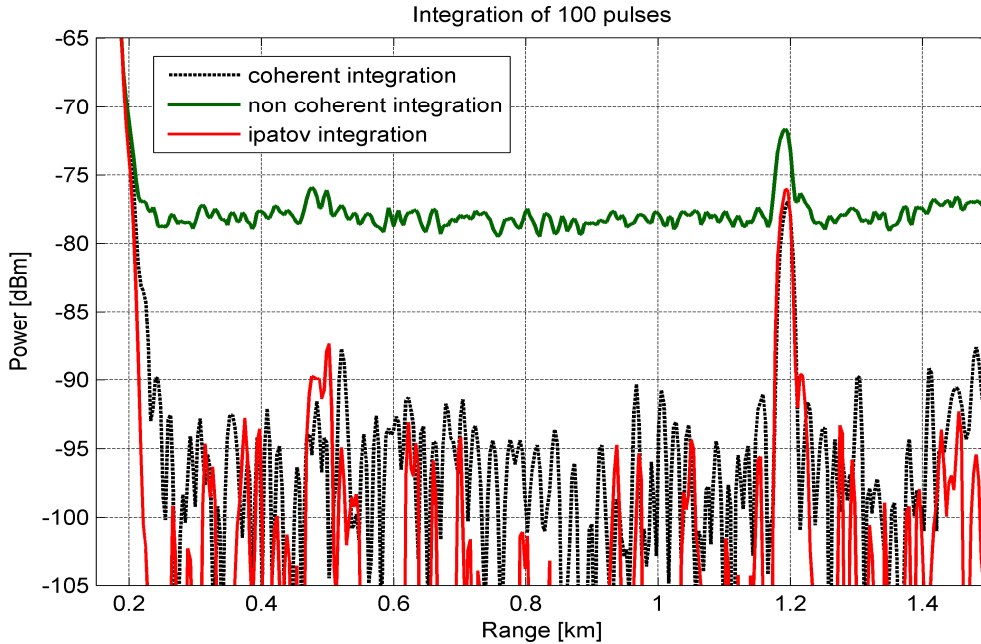


Fig. 4. Output of the three detection approaches after integration of 100 pulses (left), from a scene containing a small boat in a calm sea (right).

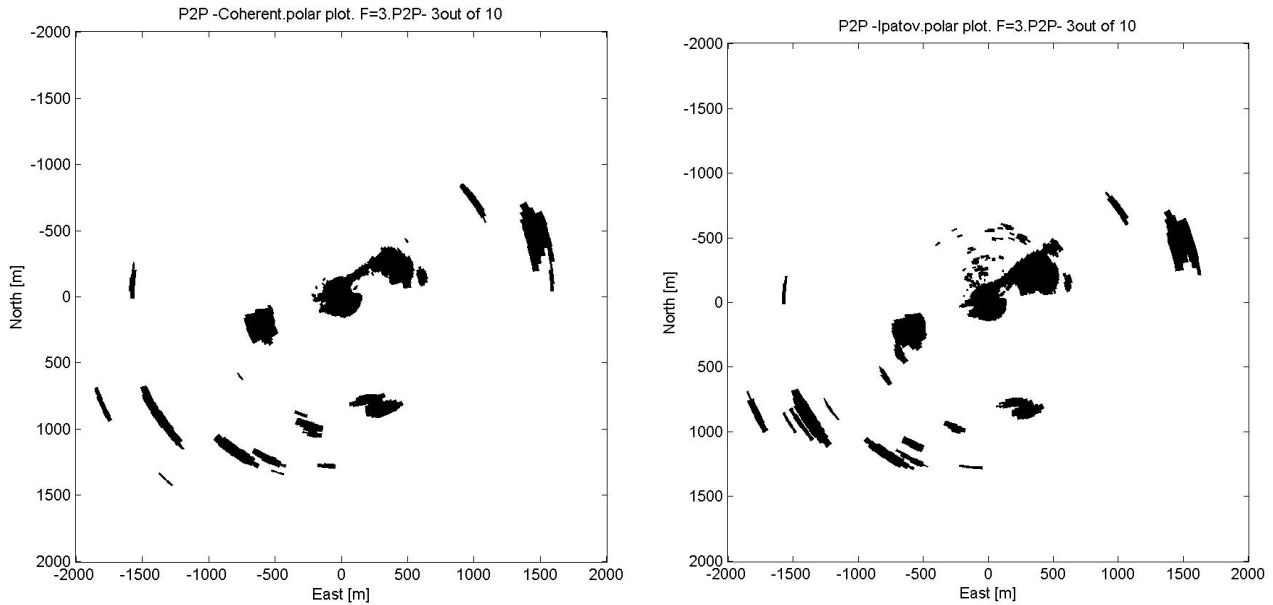


Fig. 5. Polar radar plots following CFAR and 3 out of 10 binary integration: Coherent processing (left) and Ipatov code processing (right).

The noise PDF now is more like the output of coherently integrated noise, which is Rayleigh distributed. In the Ipatov mode (red solid line) only positive values are shown.

As Fig. 4 hints, setting detection threshold for the non-coherent integration (no target) requires estimation of two parameters (e.g., mean and variance). On the other hand, the PDFs of the two other integration outputs (no target) are

specified by one parameter. This simplifies the design of an appropriate CFAR (constant false alarm rate).

We used order statistics CFAR followed by binary integration (3 out of 10 consecutive scans), to create the polar radar plots, shown in Fig. 5 (L-coherent, R-Ipatov). The results from non-coherent integration were very similar to the Ipatov processing output. The only target at sea is a small boat seen in both parts of Fig. 5 at (-1600, 100). The main

difference, in favor of coherent processing, is the shallow-water clutter, seen around (250,400) in the Ipatov (and non-coherent) processing, but not seen in the coherent processing. The nominal PRF used in this field trial was 6250Hz.

B. Ashdod Field Test

The purpose of this field trial was to test the extension of the unambiguous range by the proposed coding (Barker and Ipatov). To be able to see targets beyond the un-coded unambiguous range ($= C*PRI/2$) we needed distant large ships. The required scene is available near the port of Ashdod. The radar was located on a small dune in the southern most beach of the city of Ashdod. The port of Ashdod and the parking area of waiting ships were to the north and north-west. We also detected ships waiting to unload fuel for the power station in Ashkelon at the south.

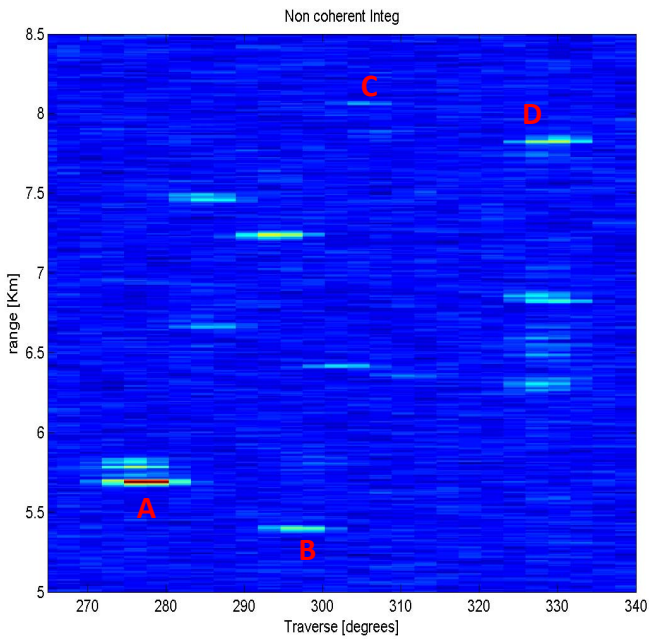


Fig. 6. Output of non-coherent processing – ships waiting to enter the port of Ashdod.

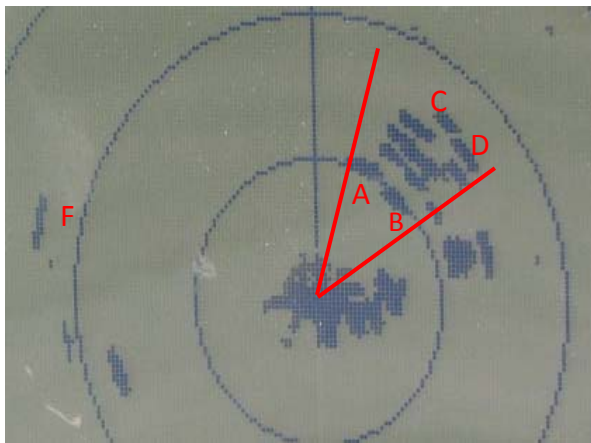


Fig. 7. Original radar display – same scene as in Fig. 6.

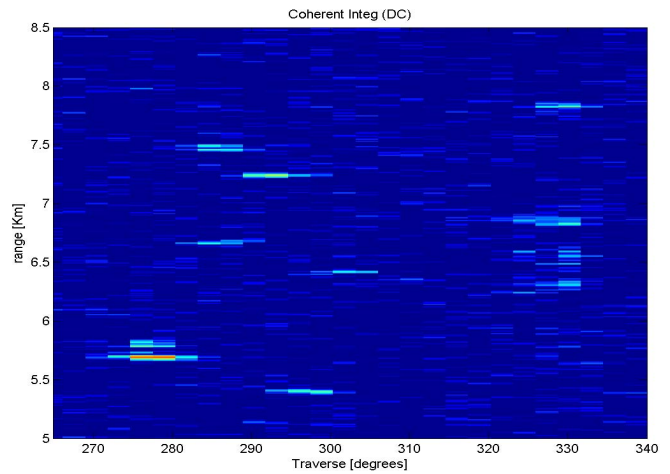


Fig. 8. Coherent processing – same scene as Fig. 6.

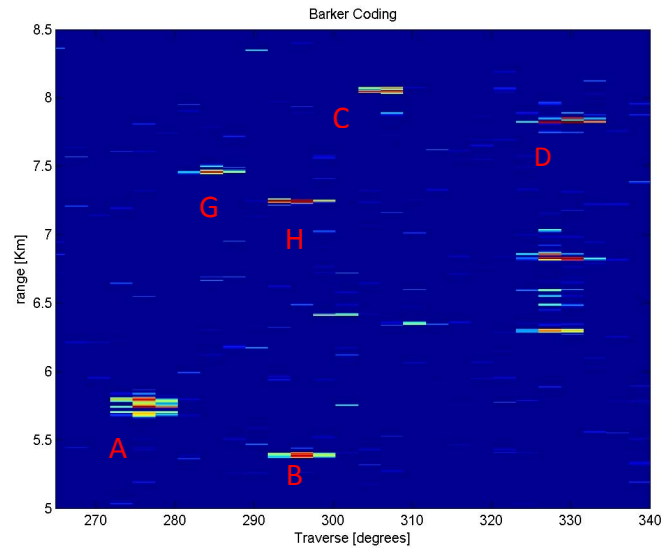


Fig. 9. Output of Barker processing – same scene as in Fig. 6 (PRF = 6250Hz).

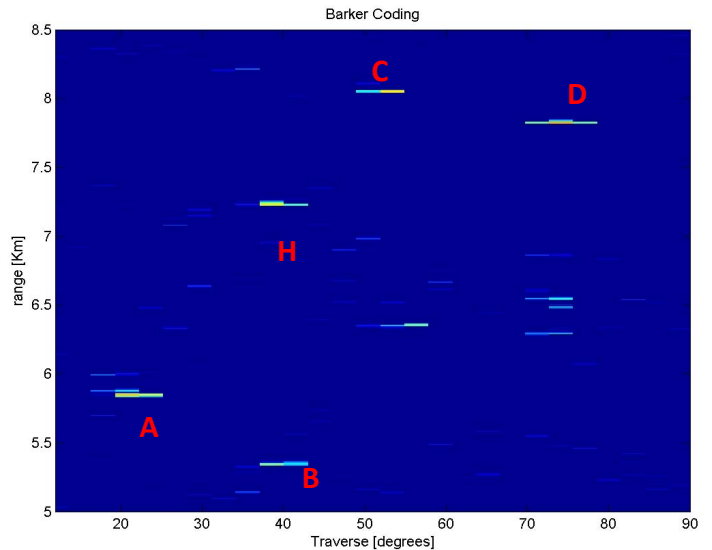


Fig. 10. Output of Barker processing – same scene as in Fig. 6 (PRF = 20000Hz).

Table 3. Transmitter parameters in the different radar operation modes.

Trans. control	PRF [Hz]	Pulse width [μ s]	Antenna rotation [rpm]	Target illumination [ms]	No. of pulse slots	% of pulses transmitted	No. of pulses trans. during illumination	Relative integrated energy on target
Built in	600	0.8	24	43.1	26	100	26	21
External	6250	0.08	41	25.2	158	50	79	6
External	12500	0.08	41	25.2	316	50	160	12
External	20k	0.08	41	25.2	500	50	250	19

Because half the pulses are not transmitted, it is hardware safe to further reduce the original shortest PRI. Instead of using the nominal shortest PRI of 0.33ms, we went down to 0.16ms and continued down as far as 0.05ms. A PRI of 0.05ms corresponds to pulse repetition frequency (PRF) of 20kHz. Without coding, PRF=20kHz implies unambiguous range of 7.5km. With coding, as in Tables 1 and 2, the corresponding unambiguous ranges become 60km and 75km respectively. The results displayed here were taken with PRF of 6250, 12500 and 20000Hz.

Figs. 6 (Cartesian coordinates) and 7 (polar coordinates) show the same group of ships waiting to enter the port of Ashdod. Fig. 6 was obtained from a single antenna scan by the external processor in its non-coherent mode. Fig. 7 is a snapshot of the radar screen created by its built-in processor. The scene in Fig. 6 occupies approximately the section marked in Fig. 7. While both processors use non-coherent detection, it is important to point out the differences. Table 3 shows that at PRF of 6250 the external mode generates only 28% of the energy on target compared to the built in mode. Figs. 8 and 9 display the same scene as Fig.6, as obtained from coherent processing and Barker coded processing.

The PRF used so far (6250Hz) corresponds to unambiguous range of 24km. Targets seen in this trial (with coded PRF) did not extend beyond 13km. In order to see how well the Barker or Ipatov coding extended the unambiguous range beyond $R=C/PRF/2$ we increased the PRF to 20kHz, corresponding to unambiguous range of 7.5km. Fig. 10 displays the same scene as Fig. 8 taken with 20kHz PRF. (The initial value of the traverse axis is not consistent from run to run.) Comparing Figs. 9 and 10, we note that target G, which appeared in Fig. 9 at a range of 7.5km, does not show up in Fig. 10. As shown in Fig. 2, the direct reception and strong near-clutter create a “hole” in the response exactly at 7.5km. The hole was deep and wide enough to conceal target G. Note that a radar at sea will not exhibit as strong and wide near-clutter as a radar on the coast, and the “hole” at $R=C/PRF/2$ will be narrower and shallower. Note that targets C and D do show up clearly despite being located beyond the nominal unambiguous range of 7.5km. In Fig. 11 the hole at 7.5km is made visible by increasing the dynamic span of the display. The additional sharp hole at 6.2km results from a hardware flaw.

We next zoom on targets A and C, obtained during the next antenna scan, 1.46s later than Fig. 10. The radial width of a pixel is 7.5m, slightly less than the 12m range resolution of a 0.08 μ s pulse. The traverse width of a pixel is 3 $^\circ$, half the horizontal beam-width of 6 $^\circ$. Because of the improved range

resolution we can tell from Fig. 12 that the bearing of ship A is nearly along the radial direction, and its length is about 180m. Fig. 13 hints that the bearing of ship C is across range and its width is about 35m. The bearing conclusions were confirmed from photos. Clearly, the radial information obtained thanks to the improved range resolution, would not be available from the original 0.8 μ s pulse (= 120m). The extent of that range resolution is marked on the two plots. Fig. 14 zooms on target A using wide pulse (0.8 μ s), constant PRF (625Hz) and non-coherent integration. The pixel width in range is 75m and the displayed target spans a range of almost 1km. Comparing Figs 12 and 14 shows that the wide pulse cannot reveal the range profile of the target but gains reflection intensity because it matches the ship’s total length. Recall that the traverse angle is correct up to a constant and changes between runs.

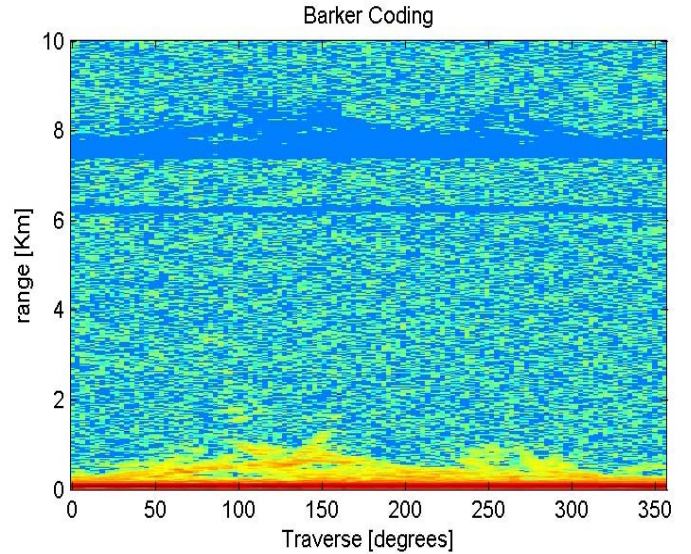


Fig. 11. The “hole” at 7.5 km.

C. Ashdod Results with CFAR and Binary Integration

Further results can be derived when the inter-pulse integration (coherent, non-coherent, Barker or Ipatov) is followed by CFAR (order statistics) detection and is then followed by inter-scan binary integration of consecutive scans (X out of 10). An example is detection of a ship near Ashkelon, at a range of 13km. The result from Barker integration is plotted in Fig. 15. The gray level of each pixel represents the number of scans X (out of 10) in which that pixel crossed the adaptive threshold. The PRF was 6250Hz.

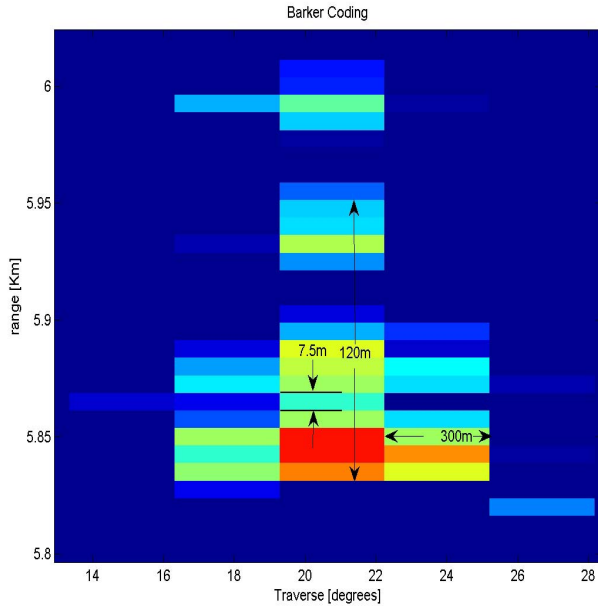


Fig. 12. Zoom on Target A.

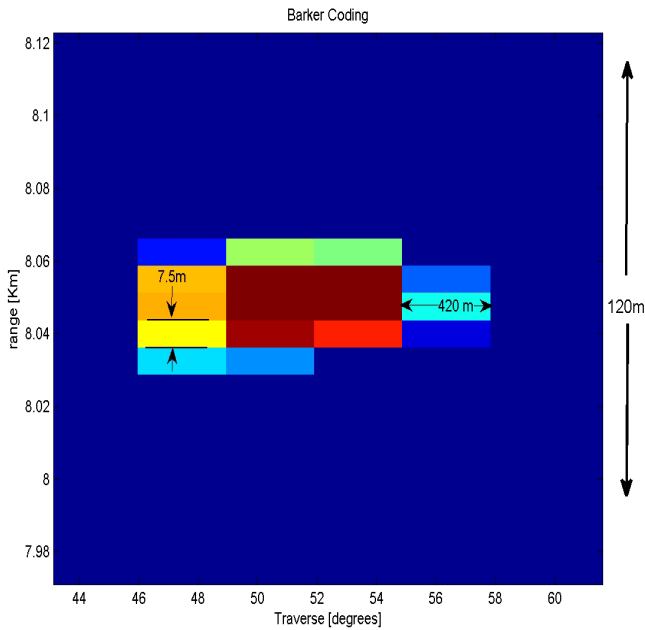


Fig. 13. Zoom on Target C.

Note that the strongest pixel at Fig. 15 was detected in 8 out of 10 scans. In non-coherent integration it was detected in all 10 scans. The detection sensitivity disadvantage of Barker (or Ipatov) processing compared to non-coherent integration is not unexpected. It can be attributed to (a) The negative elements in the Barker reference, and (b) The Hamming weight which multiplies the Barker reference. The surprising result is that following coherent integration the target at 13km was not detected even once in the 10 consecutive scans. Apparently at long distance the target/path combination degrades the pulse-to-pulse coherence.

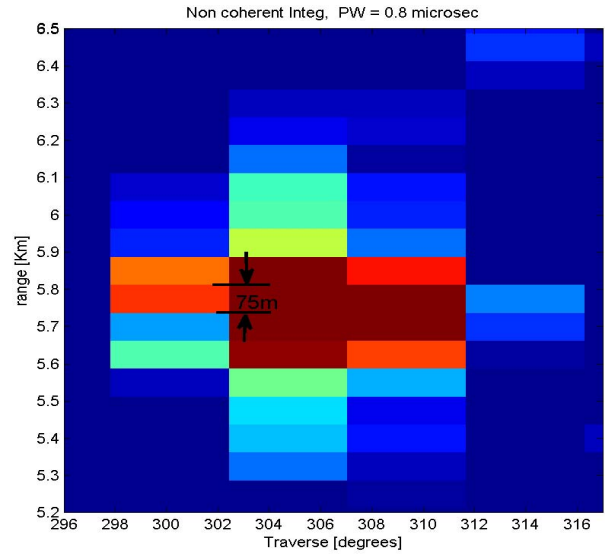


Fig. 14. Zoom on Target A with pulse width of 0.8 μ s (Non-coherent processing, PRF=625Hz).

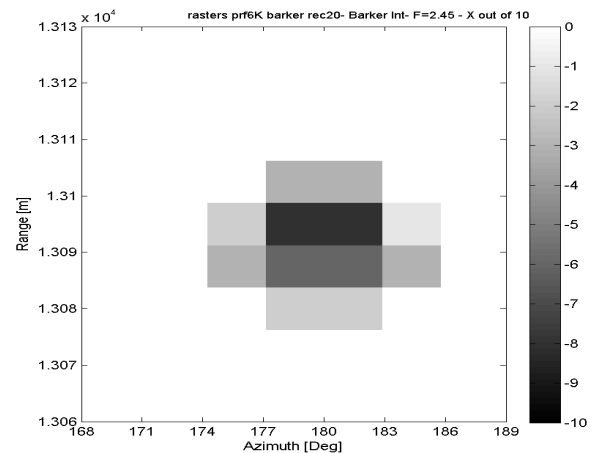


Fig. 15. Number of scans (out of 10) in which a target at 13km crosses the adaptive threshold (Barker processing, PRF=6250Hz).

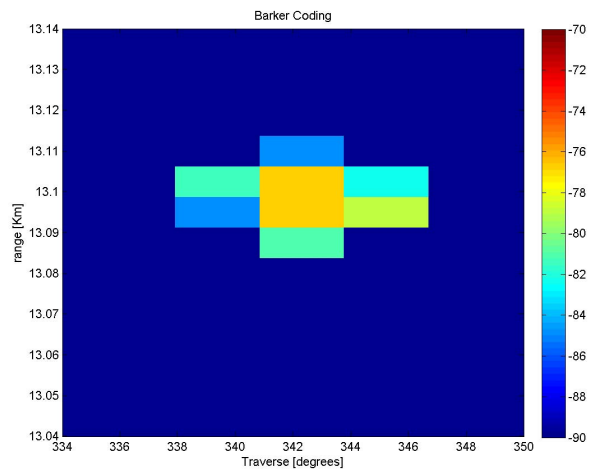


Fig. 16. Ship target at 13km (Barker processing, PRF=12.5kHz).

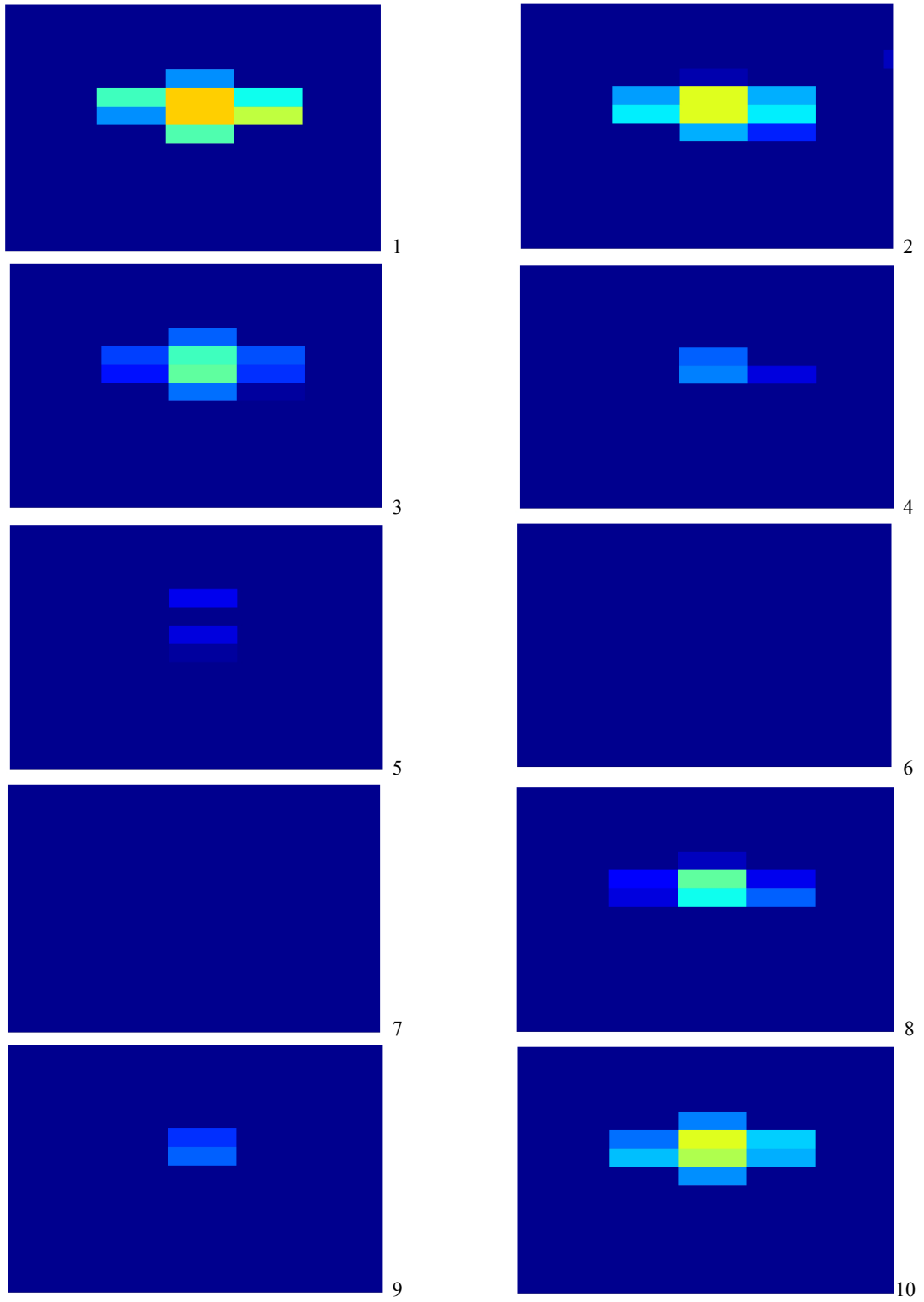


Fig. 17 Ten consecutive antenna scans of a ship target at 13.1km (PRF = 12.5kHz, Braker coded processing).

At low elevation a ship return is affected by the 90^0 corner reflector formed by the vertical hull and the sea surface [3, 4]. The long sea face of the dihedral may change from pulse-to-pulse, causing loss of coherence. In addition to pulse-to-pulse changes we note also scan-to-scan changes in target return. The nature of those can be demonstrated from 10 consecutive scans of the same ship (at 13.1km), taken with PRF=12.5kHz. At that PRF the unambiguous range is 12km, hence the ship was detected only by the coded (Barker) processing, which extends the unambiguous range. The first scan is displayed in Fig. 16, with coordinates and color bar (dB). All the 10 scans are then displayed in Fig. 17, without axis. The total duration of 10 scans is 14.6s. The 10 scans in Fig. 17 and the following 10 scans (not shown) suggest a cyclic pattern rather than random fluctuations. The radar was stationary, so a reasonable explanation is the ship’s roll. During a roll cycle the ship/water dihedral corner reflector, may sway around the optimal 90^0 angle [5]

Figs. 18 and 19 show the main advantage of coded PRI – extending the unambiguous range beyond $C/PRF/2$. At PRF=12.5kHz without coding, the direct reception and near-clutter replicate at 12km. This is evident in Fig. 18, but avoided in Fig. 19. Note the target at 13.1km, 342^0 , in Fig. 19. In Fig. 18 it may be mistaken as replicated near-clutter. The intensity of the replicated near-clutter is one fourth the original intensity, as only one out of four pulses follows a single PRI pause (see Table 1).



Fig. 20. Radar location at the Ashdod field trial.

IV. SUMMARY AND CONCLUSIONS

Our work showed that magnetron-based non-coherent radar can operate in a “narrow pulses and short PRI” mode at all ranges. This mode maintains the average power on target, required for detection, but provides better range resolution and lower clutter returns. This mode is made possible by PRI periodic coding, which extends the unambiguous range beyond the conventional $C*PRI/2$.

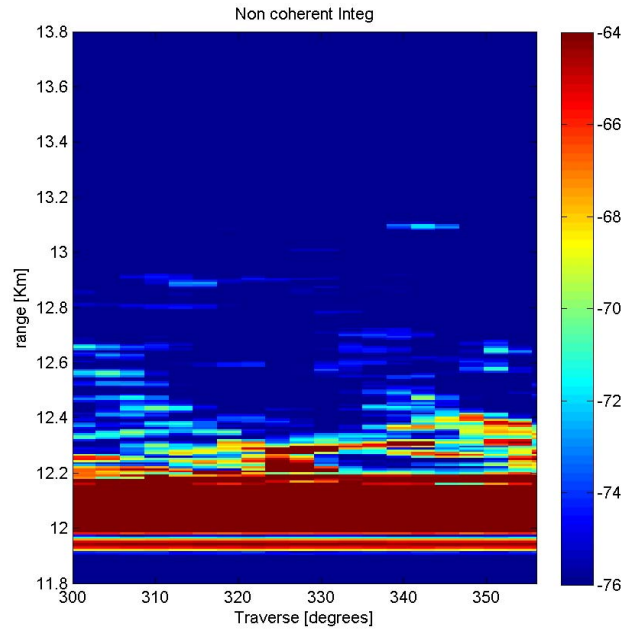


Fig. 18 Output of non-coherent integration (PRF = 12.5kHz).

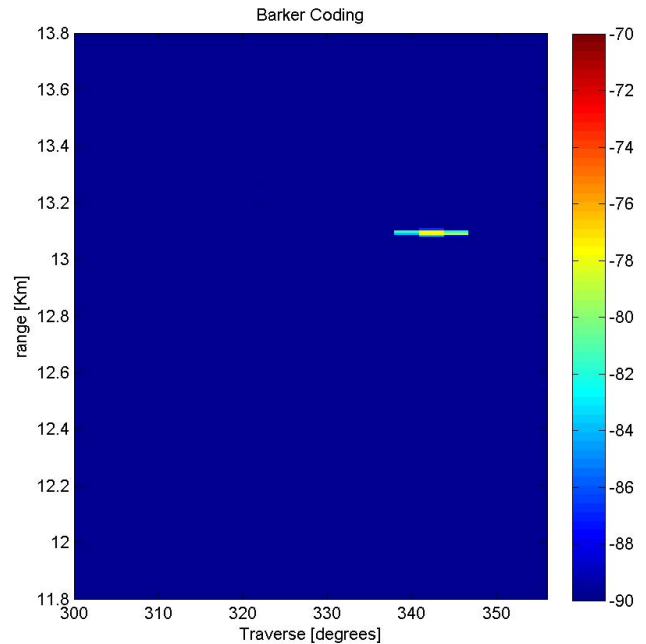


Fig. 19. Output of Barker-coded integration (PRF = 12.5kHz).

The main remaining drawback is a “hole” in the delay response at $C*PRI/2$, whose width, range-wise, depends on the width of the strong near-clutter. A remedy for that drawback is using two basic PRFs, slightly different from each other. They should be switched once per antenna revolution. The range “hole” in one antenna scan will be filled in the next scan. A target in the critical range will be seen once every two scans. We feel that the “hole” is less of a hindrance than replicated near-clutter and is also easier to fix.

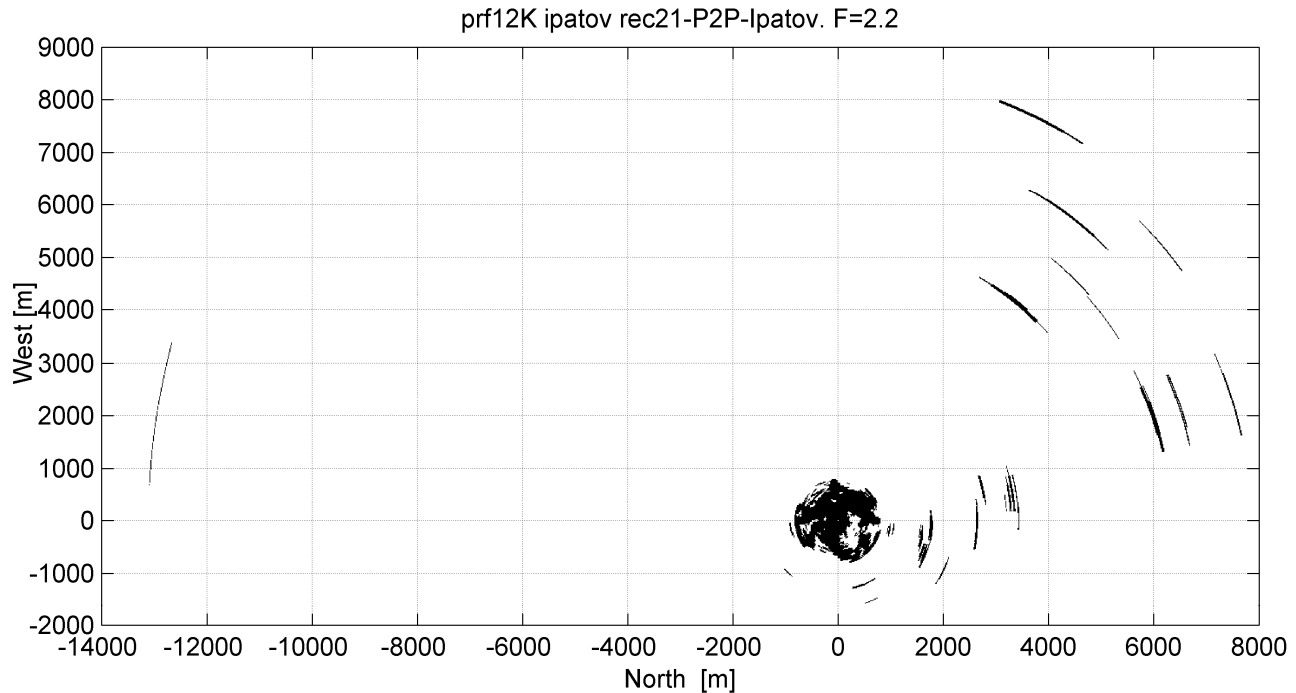


Fig. 21. Output following non-coherent Ipatov-coded processing (PRF = 12.5kHz), CFAR, and inter-scan binary integration (2 out of 10). Note 9 ships opposite Ashdod ($2 < x < 8\text{km}$, $1 < y < 8\text{km}$) and one ship opposite Ashkelon ($x \approx -13\text{km}$, $y \approx 2\text{km}$).

Field trials were performed using modified, low-cost, 2.2kW civil marine radar (FURUNO 1623). From a tripod on a beach dune mound (Fig. 20) the radar detected ships as far as 13km, with a range resolution of 12m, obtained from 80ns pulse-width. The inter-pulse coding extended the unambiguous range, e.g., in Fig. 21, beyond the nominal 12km, expected from un-coded PRF of 12.5kHz.

The modifications also included coherent-on-receive processing. Initial conclusions from comparing coherent and non-coherent processing suggest that at short-range ($< 6\text{km}$) coherent processing was advantageous, especially in reducing clutter returns. However, reflections from distant targets ($> 10\text{km}$) did not maintain pulse-to-pulse coherence, and their probability of detection by coherent integration was inferior to non-coherent integration.

One expected advantage of the proposed waveform – less clutter – was not tested in the two trials because on both days the sea was relatively calm.

ACKNOWLEDGEMENT

This work was supported by the chief scientist of the Israel Ministry of Industry, Trade and Labor. We thank the chief scientist and the technical referee Mr. S. Gabbay.

REFERENCES

- [1] N. Levanon, "New waveform design for magnetron-based marine radar," *IET Radar Sonar Navigation*, vol. 3, no. 5, pp. 530-540, October 2009.
- [2] U. Peer, and N. Levanon, "Compression waveforms for non-coherent radar", 2007 IEEE Radar Conference, Boston, MA, USA, April 17-20, 2007.
- [3] R. J. Burkholder, M. R. Pino, and F. Obelleiro, "A Monte Carlo study of the rough sea surface influence on the radar scattering from 2-D ships," *IEEE Antennas Propag. Mag.*, vol. 43, no. 2, pp. 26-33, April 2001.
- [4] R. J. Burkholder, M. R. Pino, and F. Obelleiro, "Low angle scattering from 2-D targets on a time-evolving sea surface," *IEEE Trans. Geosci. Remote Sens.*, vol. 40, no. 5, pp. 1185-1189, May 2002.
- [5] K. Jamil, and R. J. Burkholder, "Radar scattering from a rolling target floating on a time-evolving rough sea," *IEEE Trans. Geosci. Remote Sens.*, vol. 44, no. 11, pp. 3330-3337, November 2006.